The Roles of External Forcings and Internal Variabilities in the Northern Hemisphere Atmospheric Circulation Change from the 1960s to the 1990s

MARTIN P. KING

Arctic Region Supercomputing Center, and International Arctic Research Center, University of Alaska Fairbanks, Fairbanks, Alaska

FRED KUCHARSKI AND FRANCO MOLTENI*

Earth System Physics Section, Abdus Salam International Centre for Theoretical Physics, Trieste, Italy

(Manuscript received 6 May 2009, in final form 2 August 2010)

ABSTRACT

The Northern Hemisphere atmospheric circulation change from the 1960s to the 1990s shows a strong positive North Atlantic Oscillation (NAO) and a deepening of the Aleutian low. The issue regarding the contributions of external forcings and internal atmospheric variability to this circulation change has not been resolved satisfactorily. Previous studies have found the importance of tropical SST forcing. Here, this hypothesis is examined again using relatively large ensembles of atmospheric general circulation model simulations of the twentieth-century climate forced only by historically varying SST. The resulting ensemble-mean amplitude underestimates the observed change by at least 70%, although the spatial pattern is reproduced well qualitatively. Furthermore, AGCM experiments are performed to investigate other driving factors, such as the greenhouse gases, sea ice, the stratospheric ozone, as well as the contribution from atmospheric internal variability. The increase in ensemble-mean trend amplitude induced by these additional drivers was not enough to substantially improve the agreement with the observed trend. However, the full distribution of simulated trends reveals that the ensemble members at the upper tail are much closer to the observed amplitude. In the ''best'' ensemble, the 95th percentile of the simulated NAO trend amplitude remains at about 80% of the observed trend amplitude, with nearly equal contributions from external forcings and internal variability. The results also indicate that a complete set of driving factors and a correct simulation of stratospheric trends are important in bridging the gap between observed and modeled interdecadal variability in the North Atlantic winter circulation.

1. Introduction

The observed Northern Hemisphere decadal change from 1958–69 to 1985–96, which is the focus of this study, is shown in Fig. 1. (In this paper, the term ''trend'' is also used to refer specifically to this change, not a long-term trend). This spatial trend shows a strong positive North Atlantic Oscillation (NAO) and a trough in the North Pacific. The shading in Fig. 1 shows the area where the trend has a 5% significance level according to the Student's t test. Here, the significance level cannot be evaluated rigorously because, necessarily, there is only a single realization of the observed trend. The significance is calculated based on the decadal variance for December–March (DJFM). In any case, the present study focuses on the North Atlantic sector, where there is an exceptionally strong trend, providing a signal of high significance.

The connection between tropical SST forcing and extratropical circulation changes has received considerable attention (e.g., Bader and Latif 2003; Hoerling et al. 2001, 2004; Hurrell 1995; Hurrell et al. 2004; King and Kucharski 2006; Kucharski et al. 2006; Manganello 2007; Marshall et al. 2001; Mehta et al. 2000; Rodwell et al. 1999; Sutton and Hodson 2003). The warming of the tropical oceans that occurred in the last 30 yr of the twentieth century has been shown to have contributed to the observed changes in the NAO and as well in other large-scale circulation patterns (Hurrell et al. 2004). Changes in the NAO have been also connected

* Current affiliation: ECMWF, Reading, United Kingdom.

Corresponding author address: Martin P. King, School of Engineering, Monash University, Jalan Lagoon Selatan, Bandar Sunway, 46150 Petaling Jaya, Selangor, Malaysia.
E-mail: martin.p.king@gmail.com

DOI: 10.1175/2010JCLI3239.1

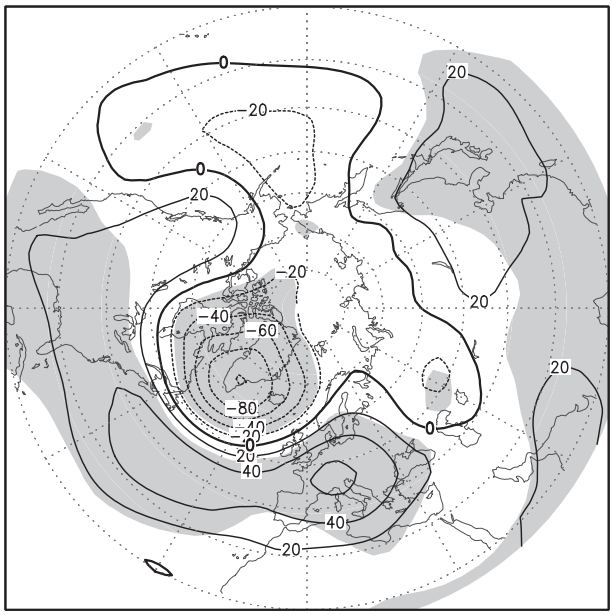

FIG. 1. Observed trend in 500-mb geopotential heights in NCEP reanalysis dataset (Kalnay et al. 1996). Contour interval (CI) = 20 m. The trend is calculated as the DJFM mean heights in the period 1985–96 minus the same in the period 1958–69. The shading indicates an area with 5% significance level.

directly to human-induced global warming (Hurrell 1995).

Although the mechanisms for tropical–extratropical teleconnection are still an active research area, fairly established dynamical understandings have emerged since the 1980s. The accepted explanation is that a tropical thermal forcing generates a stationary planetary Rossby wave train that propagates poleward and eastward. The Rossby wave perturbations also derive energy from the barotropic instability of the midlatitude basic flow in winter (Hoskins and Karoly 1981; Simmons et al. 1983; Jin and Hoskins 1995). Branstator (2002) proposes that the midlatitude circumglobal waveguide can transmit disturbances near the waveguide to distant areas. One main implication related to tropical SST–NAO teleconnection is that disturbances occurring near the South Asia jet can generate a train of waves that have the same spatial structure as the NAO in the North Atlantic. The initial lower- and upper-level responses in the tropics by the thermal forcing are explained in Gill (1980). More recent studies, such as Lu et al. (2004), Lin and Derome (2004), and Annamalai et al. (2007), provide new insights into the dynamics of tropical–extratropical teleconnection as well as on the nonlinearity of the extratropical responses.

The question regarding which part of the tropical oceans contributes most to the observed changes also receives much attention. Various studies have placed importance on the Indian Ocean (Hoerling et al. 2004; Bader and Latif 2003), western tropical Pacific Ocean (Kucharski et al. 2006), and Atlantic Ocean (Sutton and Hodson 2003; Rodwell et al. 1999).

Another well-known and important issue is the weakness of the trend amplitudes produced by all AGCMs with specified SSTs (Hurrell et al. 2004; Kucharski et al. 2006; Scaife et al. 2009). For example, Hurrell et al. (2004) reported that the 67-member multimodel global atmosphere–global ocean ensemble has a mean NAO linear trend [here defined using January–March (JFM) 500-mb geopotential heights' linear change over 1950–99] of 50 m, and the strongest trends are produced by the Community Climate Model, version 3 (CCM3) tropical ocean–global atmosphere ensemble, which has a mean NAO linear trend of 60 m. Comparing these values to the observed trend of 149 ± 42 m, as well as examining the probability density functions (PDFs) of trend amplitudes achieved among the various ensemble members (Fig. 4 of Hurrell et al. 2004), shows that the model-forced trends underestimate the observed linear trend by a factor of 2 or 3 (even larger for some models) and at the same time do not have a high likelihood of acquiring contributions from internal variability. Certain studies suggest that internal decadal variability has played a more significant role in the observed trend (Schneider et al. 2003). The simulated trend weakness is due to a number of reasons that may be broadly categorized as model or experimental design deficiencies (Hurrell et al. 2004).

The first EOF of winter (DJFM means) sea level pressure (SLP; geopotential heights can also be used) for the whole of the twentieth century has an Arctic Oscillation (AO) pattern and an increasing trend in the last two decades of the twentieth century in its principal component time series (e.g., see Fig. 2 of Shindell et al. 1999). The AO trend is only the trend in the leading EOF, whereas Fig. 1 shows a total trend defined within a particular subperiod. Shindell et al. (1999) show that a greenhouse gas forcing produces a positive AO trend; moreover, the interaction between the troposphere and stratosphere plays an important role. Further studies that support this finding include Bracco et al. (2004), Polvani and Kushner (2002), and Scaife et al. (2005). Gillett et al. (2002) reported some mixed results. On the effect of CO_2 on AO, Gillett et al. (2002) agrees with the other studies (see their Table 1, which shows a statistically significant increase in the AO index for experiments of CO_2 doubling). However, they found that a model with higher upper boundary (at 0.01 hPa with 64 vertical levels) did not obtain a stronger AO response than another model with lower upper boundary (at 5 hPa with 19 vertical levels), thus providing an opposite conclusion to Shindell

et al. (1999). In any event, subsequent studies have found that the responses are sensitive to the models, such as in gravity wave drag parameterizations (Sigmond et al. 2008), model resolutions (Polvani and Kushner 2002), and topographic heights (Gerber and Polvani 2009). The problem about the effects of stratosphere–troposphere interactions on tropospheric and surface climate responses remains unsettled (especially among models) and is a topic of active research.

Both the increased greenhouse gas and the ozone depletion radiative forcings in the second half of the twentieth century act to cool the polar winter stratosphere. This consequently strengthens the polar jet and shifts it poleward; the effect is also manifested downward to the troposphere and the earth's surface by a strengthening of the AO and the NAO (Polvani and Kushner 2002; Scaife et al. 2005; Sigmond et al. 2008). The above studies found that the ability of models to reproduce the dynamical effect of the external forcings on the stratosphere is important.

Deser and Phillips (2009) studied the roles of SST and direct atmospheric radiative forcings in the Community Atmosphere Model, version 3 (CAM3) AGCM, whereas the current study focuses on the relative roles of the external forcings and atmospheric internal variability to the NAO trend. They found that both the SST and direct atmospheric radiative forcings contribute about equally to global circulation trends. The ensemble-mean trends in the North Atlantic sector, however, were not found to be statistically significant (perhaps because of the large spread among members and the ensemble size not being big enough), with large variability among members [see Fig. 5b in Deser and Phillips (2009)].

The first aim of the current study is to assess the ensemble-mean trends and ensemble-member variabilities for experiments in which the twentieth-century historically varying SST forcing is prescribed globally and in selected oceans. In particular, the analysis focuses on the North Atlantic trend from the late 1950s to the mid-1990s, during a period when the NAO had the strongest upward trend (Fig. 2a). The ensemble sizes provided in this work exceed the sizes of most previous studies, especially for studies in which only a single model was used.

The second aim of the paper is to present results from a number of additional AGCM experiments in which the effects of CO_2, stratospheric ozone, and Arctic sea ice on the ensemble-mean trends and ensemble-member variabilities are investigated. These experiments are performed in a simplified setup in which the model is forced with climatological SST forcings defined from the periods of interest. More details are described in the following section.

The remainder of the paper is structured as follows: section 2 describes the International Centre for Theoretical Physics (ICTP) AGCM, the experimental designs for the Climate of the 20th Century (C20C) experiments, and the various idealized experiments that use SST, CO_2, sea ice, and stratospheric ozone forcings. Section 3 reports the results, a description on Taylor diagrams, and a discussion of the forced and internal variabilities using probability density functions. Lastly, the concluding remarks are given in section 4.

2. Descriptions of the AGCM and experimental designs

The ICTP AGCM, which has a spectral resolution T30 and eight vertical levels, is used. The parameterized processes are described fully in the appendix of Molteni (2003). The two topmost layers approximate the stratosphere (some features are described in section 3b). It is a later version of ICTP AGCM, described originally in Molteni (2003) (additional validations can be found online at http://users.ictp.it/~kucharsk/speedy8_clim.html). Examples of previous papers relevant to the current study employing this model are Bracco et al. (2004), who studied the atmospheric climate variability in a number of Northern Hemisphere sectors forced by SST and CO_2; Kucharski et al. (2006) focused on the forcing of NAO decadal changes by tropical SSTs; and Sterl and Hazeleger (2005) focused on the effects of tropical and extratropical SSTs to the internal variability of the atmosphere.

a. C20C experiments

The following four selected sets of experiments are used to investigate the connection between SST variations and the atmospheric responses in the model:

- **Global Ocean–Global Atmosphere (GOGA)**: 100-member ensemble with globally prescribed observed SST from 1870 to 2002.
- **Tropical Ocean and Global Atmosphere (TOGA)**: 10-member ensemble with prescribed observed SST from 1870 to 2002 in the whole tropical belt (20°S–20°N).
- **Tropical Indo-Pacific Global Atmosphere (TIPGA)**: 10-member ensemble with prescribed observed SST from 1870 to 2002 tropical Indo-Pacific region (from the eastern coast of Africa to the western coast of South America and 20°S to 20°N).
- **Tropical Pacific Global Atmosphere (TPAGA)**: 10-member ensemble with prescribed observed SST from 1870 to 2002 in the tropical Pacific region (from 130°E to the western coast of South America and 20°S–20°N).

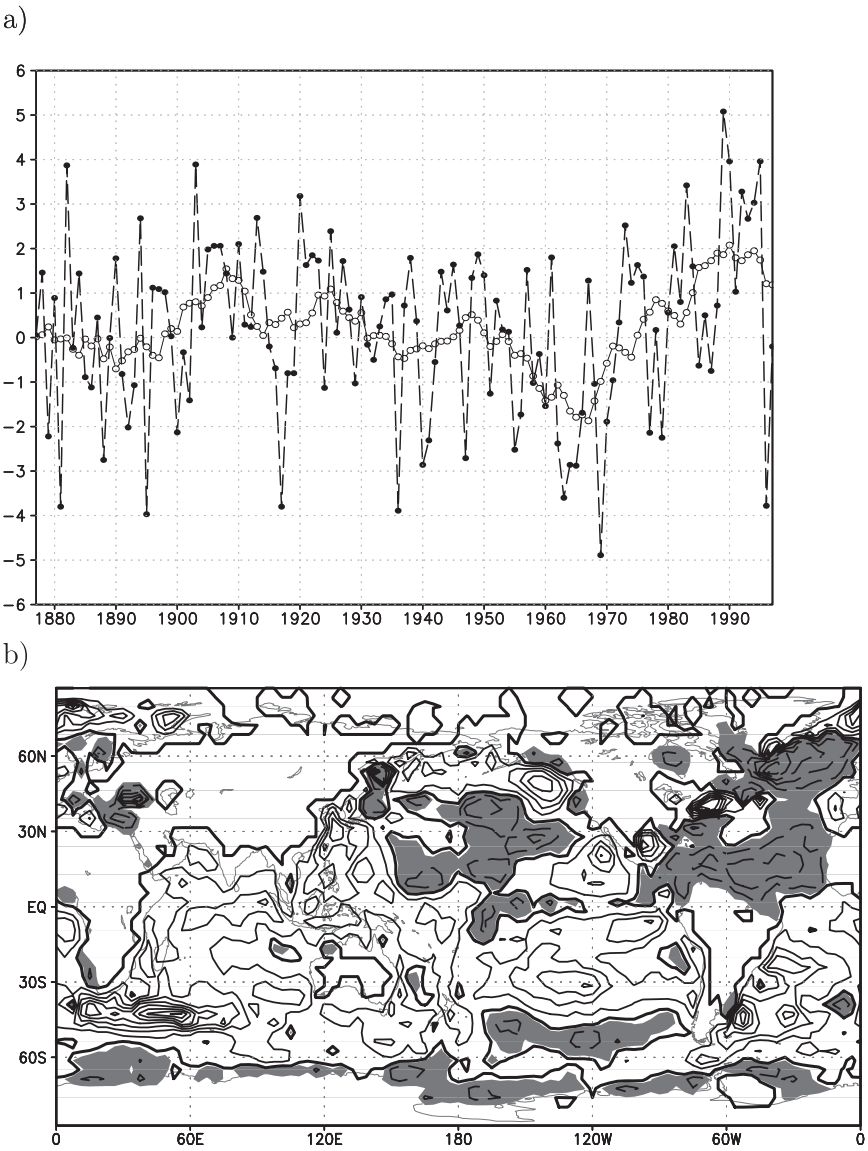

FIG. 2. (a) Time series of the DJFM NAO index (dashed line) and its 11-yr running mean (solid line); (b) DJFM SST trend (1985–96 minus 1958–69) in HadISST. Negative values are shaded. CI = 0.2 K.

In ocean regions where SST anomalies are not specified, climatological SST is prescribed, except for the North Atlantic basin, where SST anomalies are calculated using a 50-m thermodynamic slab ocean model to include the effect of local atmosphere–ocean feedback in the North Atlantic region. The sets of experiments above are summarized in Table 1. All of the ensembles use SST from the Met Office Hadley Centre Sea Ice and Sea Surface Temperature (HadISST) dataset (Rayner et al. 2003).

For each ensemble, different members are created by randomly perturbing the initial conditions and by performing a 1-yr spin-up integration. The intraensemble variability is used to estimate the statistical significance of the responses.

b. *Idealized experiments with "climatological" SST forcings*

For these experiments, the strategy is essentially similar to that used by Manganello (2007) and Schneider et al. (2003). Climatological SST fields that are being used to force the model are calculated from the observed SST for the selected periods of 1958–69 or 1985–96. These forcing climatological SSTs vary from month to

TABLE 1. Summary of C20C experimental setups. The SST anomalies are added to the global climatological SST field in the C20C experiments.

Expt	Definition region for SST anomaly	Ensemble size
GOGA	Globally	100
TOGA	Whole tropical belt, from 20°S to 20°N	10
TIPGA	Coast of Africa to coast of South America, from 20°S to 20°N	10
TPAGA	130°E to coast of South America, from 20°S to 20°N	10

month (interpolated to vary day to day by the model), but there is no interannual variation in any of the external forcings (including, of course, the SSTs).

The main advantage of this type of experimental setup is that large samples of a season can be obtained quickly. Schneider et al. (2003) argued that this technique is useful, especially for investigating decadal responses in which the atmosphere has a long time to reach a quasi-equilibrium state. All experiments for this section are run for either 200 or 300 model years. Because of the relatively long runs as well as the higher trend amplitudes obtained in most cases, all trends shown here have been found to be statistically significant.

An experiment is labeled with "EXP(·)," where the forcing SST defined for a particular period used is shown within the parentheses. If there is another parameter in the AGCM that is changed (i.e., different from the default values) in a particular experiment, it is also indicated within the parentheses. As an example, EXP(hsst1958–1969) labels an experiment forced with climatological SST calculated from observed SST in the years 1958–69 using the HadISST dataset. Table 2 lists the experiments discussed in section 3b.

To investigate responses to a different SST dataset, the National Oceanic and Atmospheric Administration (NOAA) SST (Smith and Reynolds 2004) is also used. Experiments with changes in atmospheric CO_2 and stratospheric ozone in ICTP AGCM are also performed. Finally, the effect of sea ice is investigated briefly using ICTP AGCM coupled to a simple sea ice thermodynamic column model following Bitz and Lipscomb (1999).

In ICTP AGCM, the two parameters that are related to CO_2 and stratospheric ozone radiative forcings are named α_{CO2} and EPSSW, respectively. Increasing the value of α_{CO2} from its default would result in a decrease in the longwave transmissivity (i.e., more longwave absorption), and decreasing the value of EPSSW from its default would result in a decrease in the absorption of incoming solar radiation in the stratosphere [see appendix of Molteni (2003)]. Because the mathematical relationships of these parameters in this model to the concentrations of CO_2 and ozone in the real atmosphere are not known, we decide on the appropriate values based on the global-averaged annual-mean radiative forcings that would result. For the experiments using stratospheric ozone radiative forcing, the zonal-mean wind trend in the stratosphere produced is also used to judge if the value of EPSSW used in an experiment is suitable.

In the experiments presented in the current study, the value of α_{CO2} is changed from 5 to 6, to represent an increase in CO_2 over the second half of the twentieth

TABLE 2. Summary of the idealized experiments. All SST fields are applied globally. The acronyms hsst and hice refer to SST and sea ice fraction, respectively, from the HadISST dataset (Rayner et al. 2003); nsst refers to SST from Smith and Reynolds (2004); α_{CO2} is the absorptivity coefficient in longwave radiation by CO_2 (default value = 5); EPSSW is related to the absorption of incoming solar radiation by ozone in the stratosphere (see section 3b); SO is a 50-m slab ocean model in the Northern Hemisphere; and SICE refers to the Bitz and Lipscomb (1999) sea ice model described in section 3b. The experiment marked with an asterisk is considered to have the best-scenario forcings.

Expt	SST	Sea ice	α_{CO2}	EPSSW	SO	SICE
EXP(hsst1958–69)	hsst(1958–69)	hice(1958–69)	5	0.025	No	No
EXP(hsst1985–96)	hsst(1985–96)	hice(1985–96)	5	0.025	No	No
EXP(hsst1985–96, α_{CO2} = 6)	hsst(1985–96)	hice(1985–96)	6	0.025	No	No
EXP(nsst1958–69)	nsst(1958–69)	hice(1958–69)	5	0.025	No	No
EXP(nsst1985–96)	nsst(1985–96)	hice(1985–96)	5	0.025	No	No
EXP(nsst1985–96, α_{CO2} = 6)	nsst(1985–96)	hice(1985–96)	6	0.025	No	No
EXP(nsst1958–69, SISO)	nsst(1958–69)	hice(1958–69)	5	0.025	Yes	Yes
EXP(nsst1985–96, α_{CO2} = 6, SISO)	nsst(1985–96)	hice(1985–96)	6	0.025	Yes	Yes
EXP(nsst1985–96, α_{CO2} = 6, EPSSW = 0.023)	nsst(1985–96)	hice(1985–96)	6	0.023	No	No
EXP(nsst1985–96, α_{CO2} = 6, EPSSW = 0.021)	nsst(1985–96)	hice(1985–96)	6	0.021	No	No
EXP(nsst1985–96, α_{CO2} = 6, EPSSW = 0.019)	nsst(1985–96)	hice(1985–96)	6	0.019	No	No
EXP(nsst1985–96, α_{CO2} = 6, EPSSW = 0.02, SISO)*	nsst(1985–96)	hice(1985–96)	6	0.02	Yes	Yes
EXP(nsst1958–69, hice1958–69, SI)	nsst(1958–69)	hice(1958–69)	5	0.025	No	Yes
EXP(nsst1958–69, hice1985–96, SI)	nsst(1958–69)	hice(1985–96)	5	0.025	No	Yes

century. If linearity is assumed for a small change, then this translates to a 20% increase in CO_2, which is consistent with its change in the second half of the twentieth century (Forster et al. 2007). Estimation of the resulted annual-mean global-averaged radiative forcing in ICTP AGCM by the methods of ''instantaneous surface radiative forcing'' and ''zero surface-temperature-change radiative forcing'' [see section 2.2 of Forster et al. (2007)] found values between 1 and 1.5 W m^{-2}. These numbers are also consistent with the observed change and values produced in other climate models (Forster et al. 2007).

3. Results and discussions

a. C20C experiments

The focus here is on the North Atlantic part of the hemispheric trend. The observed DJFM NAO index (dashed line with filled circles) and the decadal NAO index (solid line with open circles; after applying an 11-yr running mean) are shown in Fig. 2a (using data available online at http://www.cgd.ucar.edu/cas/jhurrell/nao.stat.winter.html). The NAO change between the two 12-yr periods of 1958–69 and 1985–96, approximating, respectively, the periods with the lowest and highest decadal NAO values, is referred to here as the trend. Figure 2b shows the observed trend in global SST in the HadISST dataset. The most striking feature is the ocean warming of the Pacific Ocean and Indian Ocean of about 0.5 K. Cooling of sea surface temperatures occurs in the subtropical North Atlantic and the subtropical North Pacific.

Figures 3a–d show the 500-hPa height trends for the ensemble means of the GOGA, TOGA, TIPGA, and TPAGA experiments, respectively (these results are described below in parallel using Taylor diagrams in Fig. 4). The shading indicates the region where the anomaly has 5% significance level. The observation (Fig. 1) shows a strong positive NAO trend with amplitudes of 80 and 40 m of the northern and southern NAO centers, respectively. A weaker trough occurs in the North Pacific. For the model integrations, the statistical significance is estimated from the variance of trends among individual ensemble members, which results from internal atmospheric variability, since all members have the same SST forcing.

To summarize the ensemble variability and performance effectively, Taylor diagrams (Taylor 2001) are used. Figures 4a–d show the Taylor diagrams for 500-hPa height trends calculated for the North Atlantic region (30°–85°N, 90°W–60°E) for GOGA, TOGA, TIPGA, and TPAGA experiments, respectively.

The interpretation of a Taylor diagram is described briefly here. We use an open triangle to represent the observed trend, a solid square for the ensemble-mean trend, and solid dots for the members' trends. The ensemble-mean trend is also the forced trend because the internal variability is cancelled by the ensemble averaging. The radial distance (defined as $r = |\mathbf{T}_j|/|\mathbf{T}_O|$) from the origin to a point indicates the spatial amplitude of a particular trend $|\mathbf{T}_j|$ normalized by the spatial amplitude of the observed trend $|\mathbf{T}_O|$. Thus, a point close to the unit circle represents a spatial trend with a similar amplitude to the observed spatial trend. The cosine of the azimuthal angle α of a point [defined as $\cos(\alpha) = \mathbf{T}_j \cdot \mathbf{T}_{\rm EM}/|\mathbf{T}_j||\mathbf{T}_{\rm EM}|$] indicates the spatial correlation of a particular trend $\mathbf{T}_j$ with the ensemble-mean trend $\mathbf{T}_{\rm EM}$. Thus, for example, the lower the triangle is, the better the observed trend and the ensemble-mean trend resemble each other. Note that r and α are defined independently from each other.

It is easily shown that $x = \mathbf{T}_j \cdot \mathbf{T}_{\rm EM}/|\mathbf{T}_O||\mathbf{T}_{\rm EM}|$. There is a special case of $x = \cos(\alpha)$ for $\mathbf{T}_j = \mathbf{T}_O$, meaning that the spatial correlation between the observed and the ensemble-mean trends is just the x coordinate of the triangle. Our usage of the Taylor diagram is slightly unconventional in that the ensemble-mean trend, rather than observed trend, is used as the reference field in defining α. The reason for this usage is that the observed trend may be viewed as one realization among many possible events and thus it is regarded as one special member of the ensemble. Another published study that uses the Taylor diagram in this way is Kucharski et al. (2009).

In general, we look for the following features in a Taylor diagram:

(i) low triangle (meaning a large spatial correlation between ensemble-mean and observed trends) and
(ii) square as close to $x = 1$ as possible (i.e., ensemble-mean trend having an amplitude as close as possible to the observed trend amplitude, so the trend is highly predictable) *or* having enough proportion of dots (the ensemble members) reaching at least $r = 1$ (this means that if the ensemble-mean trend amplitude is not high enough, then at least the variability among members explains the observed trend amplitude).

The Taylor diagrams in Fig. 4 show that ensemble-mean trends in GOGA and TOGA (Figs. 3a,b) resemble closest the observed trend (indicated by the ''low'' triangles). The trend in the North Atlantic region is NAO like (the centers are slightly shifted to the southwest). The spatial correlations of the ensemble-mean trend with the observed trend are 0.57 for GOGA and 0.76 for TOGA over the North Atlantic region (30°–85°N, 90°W–60°E).

The model captures only about 20% of the observed amplitude (TOGA has slightly larger amplitudes than GOGA). These results suggest that the effect of the prescribed extratropical SST anomalies in GOGA is small, but it acts to slightly weaken the flow anomalies forced by the tropical SSTs and reduces the spatial

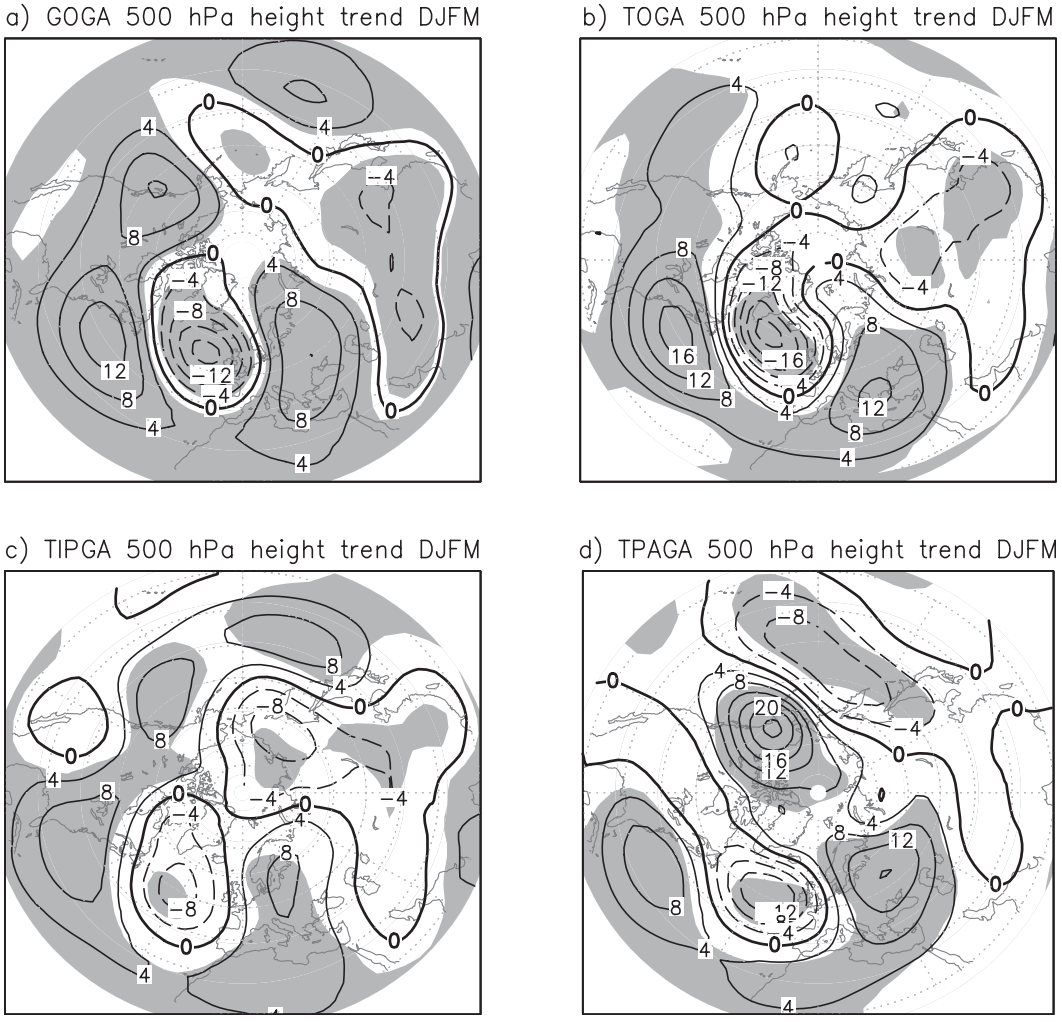

FIG. 3. The DJFM 500-hPa height 1985–96 to 1958–1969 trends: (a) GOGA, (b) TOGA, (c) TIPGA, and (d) TPAGA ensemble means. CI = 4 m. Shading indicates an area with 5% significance level.

correlations of the trends with observation. TIPGA and TPAGA show similar responses, but they have less resemblance with the observed trend (spatial correlations of 0.54 and 0.2, respectively).

In Fig. 4b, the spatial amplitude of the TOGA ensemble-mean trend is only about 20%–30% of the spatial amplitude of the observed trend, but the amplitudes of some member trends (radial distances of solid dots) can reach about 50% of the amplitude of the observation. There is, however, no trend among the ensemble members, which has the same amplitude as the observed trend.

The inclusion of the Indian Ocean in the TIPGA ensemble has improved over TPAGA in terms of the spatial correlation of the ensemble-mean with the observed trends. However, it was found that an ensemble forced with the Indian Ocean alone resulted in very low trend correlation and amplitude in the ICTP AGCM (not shown here). In additional experiments, we also find that no other isolated tropical ocean basin ensemble performed as well as the TOGA ensemble.

It is usually not straightforward to identify which tropical ocean basin has a more significant role in forcing the NAO trend (see previous studies cited in the introduction), nor is it straightforward to analyze how the combined effect on the trend results from the independent role of each tropical ocean basin. We note, however, that the results given in Fig. 4 are consistent with previous findings (e.g., Hurrell et al. 2004; Deser and Phillips 2009), which conclude that in AGCM experiments that are forced by observed SST fields only, the Northern Hemisphere general circulation change is driven mainly by the tropical SST.

The underestimation in the trend amplitude is a weakness shared by many models, including both AGCMs and

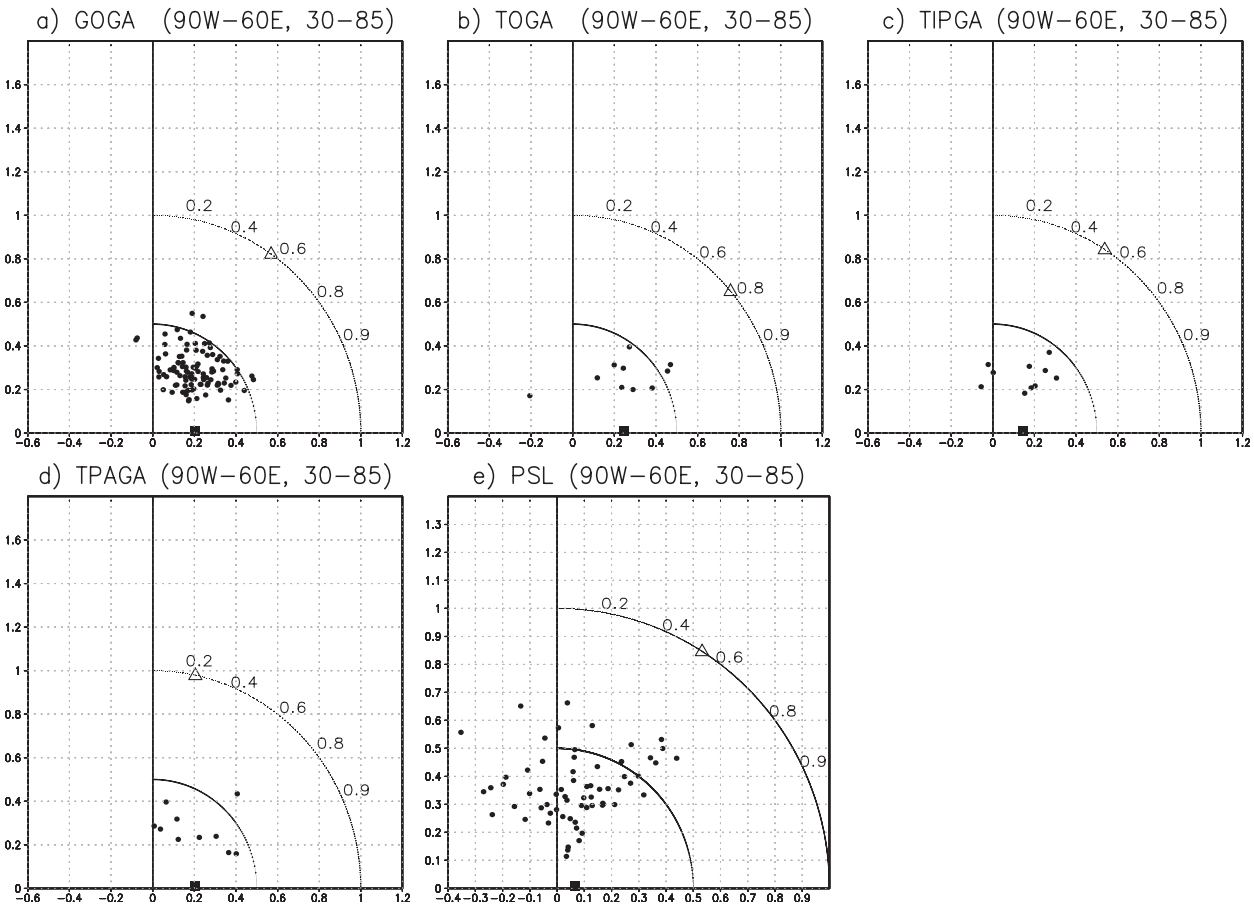

FIG. 4. For the respective ensemble labeled, each panel shows a Taylor diagram for the 500-hPa height trends in the North Atlantic region (30°–85°N, 90°W–60°E) from 1958–69 to 1985–96. Ensemble members (solid dots) are compared with the NCEP reanalysis trend (triangle) and ensemble-mean trend (square). (e) Results of North Atlantic PSL linear trends from 65 CMIP3's 20C3M experiments (see text). See section 3a for an explanation of Taylor diagram.

coupled models (Hurrell et al. 2004; Scaife et al. 2009). Shown in Fig. 4e is the Taylor diagram for North Atlantic SLP linear trends from 1950 to 1999 by 65 Intergovernmental Panel on Climate Change (IPCC) Coupled Model Intercomparison Project phase 3 (CMIP3) model integrations (from the 20C3M experiments). Similarly, the weak trend amplitudes are observed among these members. What may be more worrying is the large proportion of the members that have negative spatial correlations with the observed trend (inferred as some of those which lie in the left quadrant in the Taylor diagram, because the ensemble-mean trend has a positive spatial correlation with the observed trend). Deser and Phillips (2009) found that in the Community Climate System Model, version 3 (CCSM3) coupled model, the problem is caused by the model's inability to reproduce the historical SST in experiments in which a range of radiative forcings were prescribed. This may be a common issue among the CMIP3 models.

b. Idealized experiments

1) EFFECTS OF CO_2, SEA ICE, AND STRATOSPHERIC OZONE

This section presents results from experiments described in section 2b. As in the previous section, the focus is on the North Atlantic sector (30°–85°N, 90°W–60°E). Visual comparison of the behavior in the Aleutian low is also carried out.

The main aim of these experiments is to investigate and identify the effects of some other potential drivers, besides SST, for the observed atmospheric trend discussed in this paper. The set of experiments presented here are summarized in Table 2.

Comparing with the observed trend in Fig. 1, Figs. 5a,c show that experiments using the global SST forcings (defined from HadISST or NOAA SST reanalysis datasets) alone do not produce satisfactory trend patterns and amplitudes. The Taylor diagrams for these four

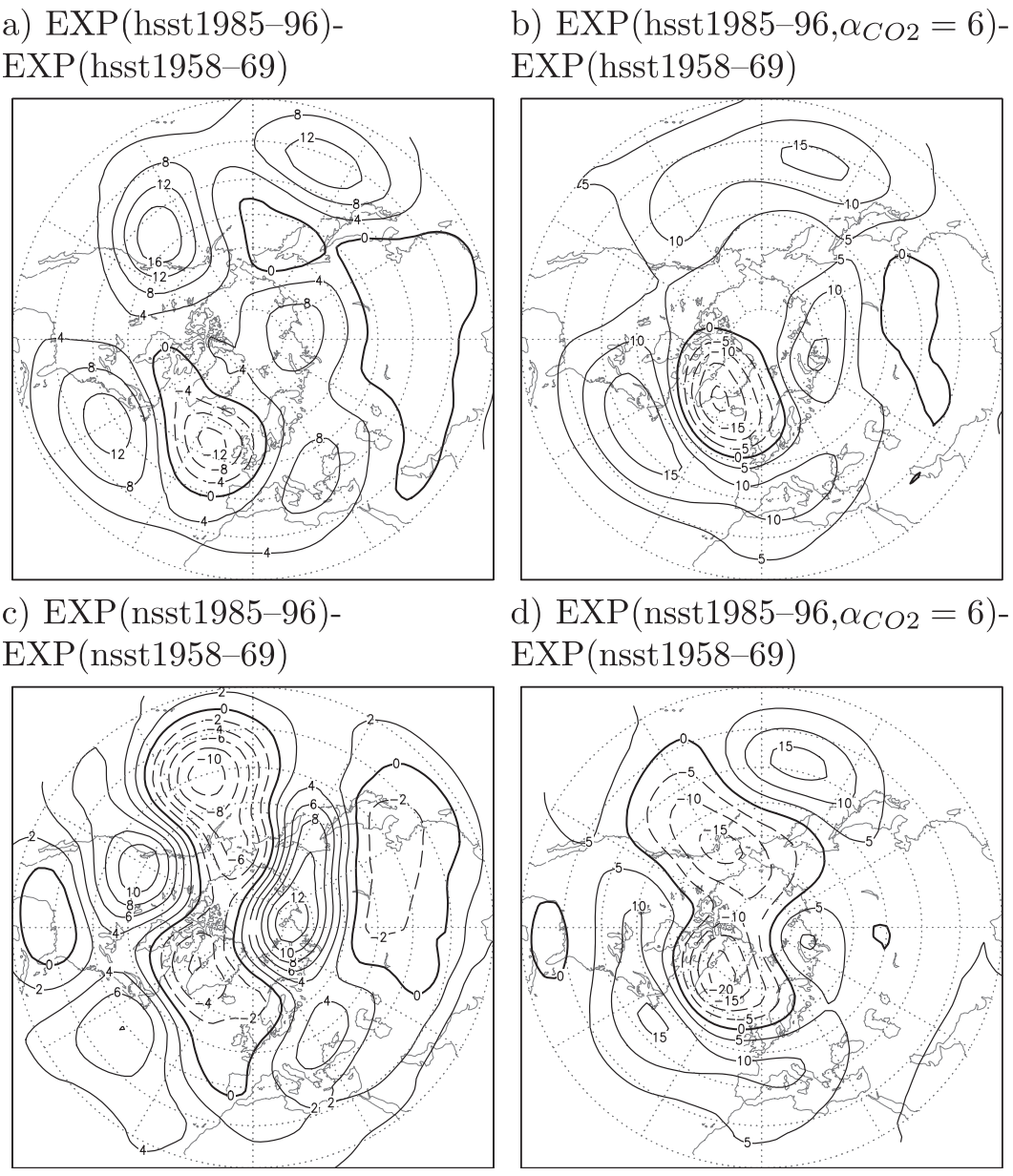

FIG. 5. DJFM 500-mb-mean geopotential heights trends. If not indicated, $\alpha_{CO2} = 5.0$ (the default value). CI = (a) 4, (b) 5, (c) 2 and (d) 5 m.

experiments are shown in Fig. 6. Each trend ''member'' (solid dots) is the trend found in a randomly selected pair of geopotential height fields in DJFM from the two experiments concerned. We sample enough pairs to give a clear indication of the ''clouds'' of members. The Taylor diagrams in Figs. 6a,c indicate low ensemble-mean and member amplitudes, as well as fairly low spatial correlations of the ensemble means with the observed trend.

The trends shown in Figs. 5b,d are obtained by experiments with an increase in CO_2 in the later period of 1985–96. The parameter α_{CO2} is the longwave (around 15 μm) absorptivity coefficient by CO_2 in the radiation scheme of ICTP AGCM [described in detail in the appendix of Molteni (2003)]; its default value is tuned to 5.0. The CO_2 longwave absorptivity coefficient of $\alpha_{CO2} = 6.0$ produces a global-averaged annual-mean radiative forcing of about 1 W m^{-2} in this model that is close to the estimated change in the last few decades of the twentieth century (Forster et al. 2007, p. 208).

The Taylor diagrams in Fig. 6 indicate that the mean trends (shown in Fig. 5) are able to reproduce, at best, about 20%–30% of the observed trend amplitudes. The

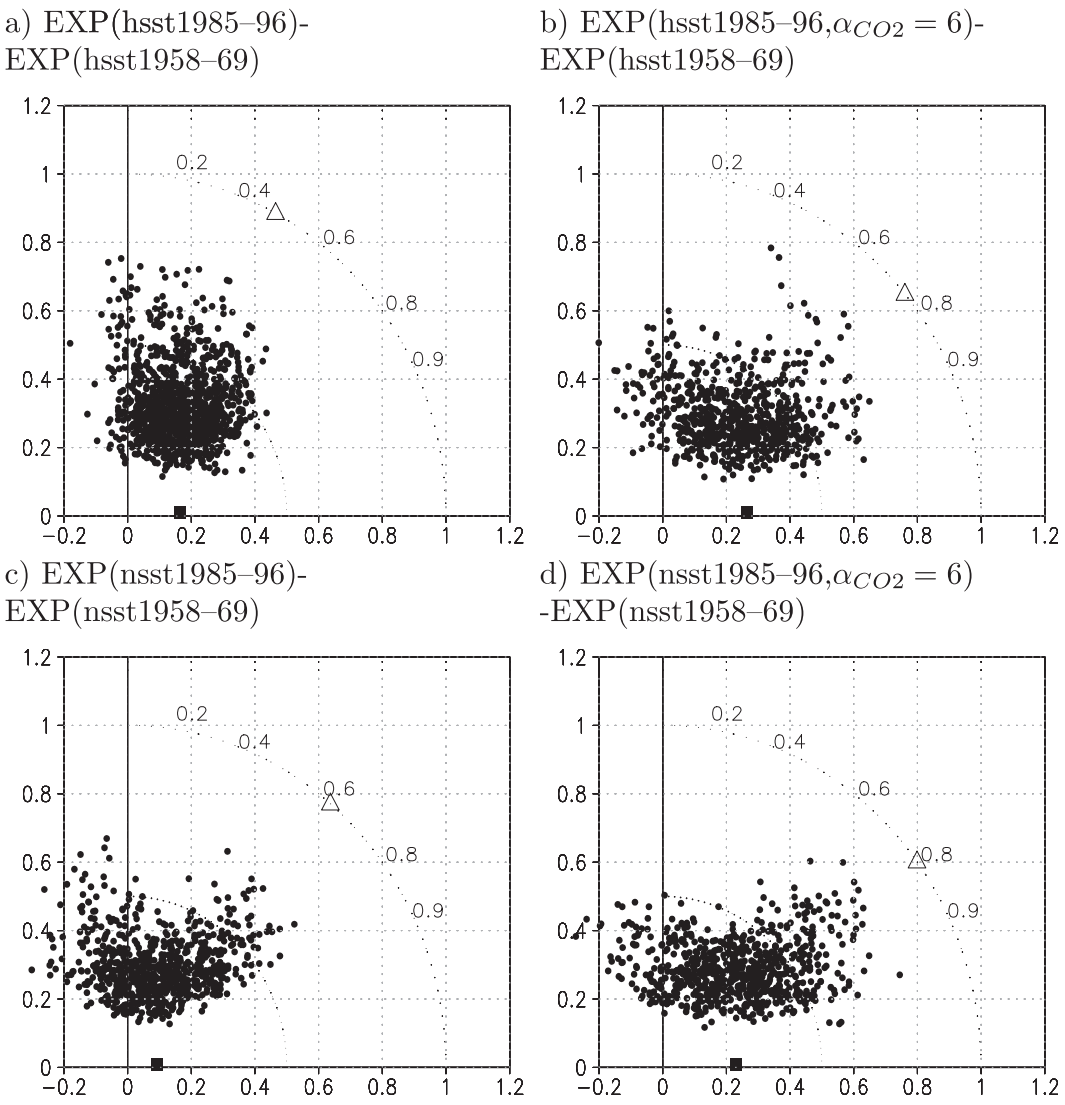

FIG. 6. Taylor diagrams for DJFM 500-mb geopotential heights trends of the ensemble members. If not indicated, $\alpha_{CO2} = 5.0$. Open triangle represents observed trend, solid square the ensemble-mean trend (i.e., for the respective trend shown in Fig. 5), and the solid dots the members trends. Taylor diagrams are calculated for 30°–85°N, 90°W–60°E.

NOAA SST produces trends with slightly better spatial correlations with the observed trend (the triangles for NOAA experiments are lower); experiments forced with a change in CO_2 also perform better in both amplitudes and spatial correlation of the trends. The differences in the responses from the HadISST and NOAA SSTs are probably due to the slightly more widespread area of warming in the equatorial pacific for the NOAA SST (not shown here). Taking Fig. 6d as an example, it is seen that there are a few trend members that can achieve up to 80% of the observed trend amplitudes. The spatial correlation between the observed and ensemble-mean trend is, however, very high at 0.8. The spatial trend in Fig. 5d also shows a strengthening of the Aleutian low in the North Pacific, although its location is not accurate.

For all of the ICTP AGCM experiments presented in this study, the proportion of members with negative spatial correlations (those in the left quadrant in the Taylor diagram) is small. They also have small correlations (lying near $\alpha = 90°$) as well as small normalized amplitudes relative to members to the right.

Figure 7a shows the percentage of members with normalized trend amplitudes greater than the values indicated on the x axis: Less than 10% of the members achieved normalized amplitudes of at least 0.7, and 0% over 0.82. This shows that even allowing the natural

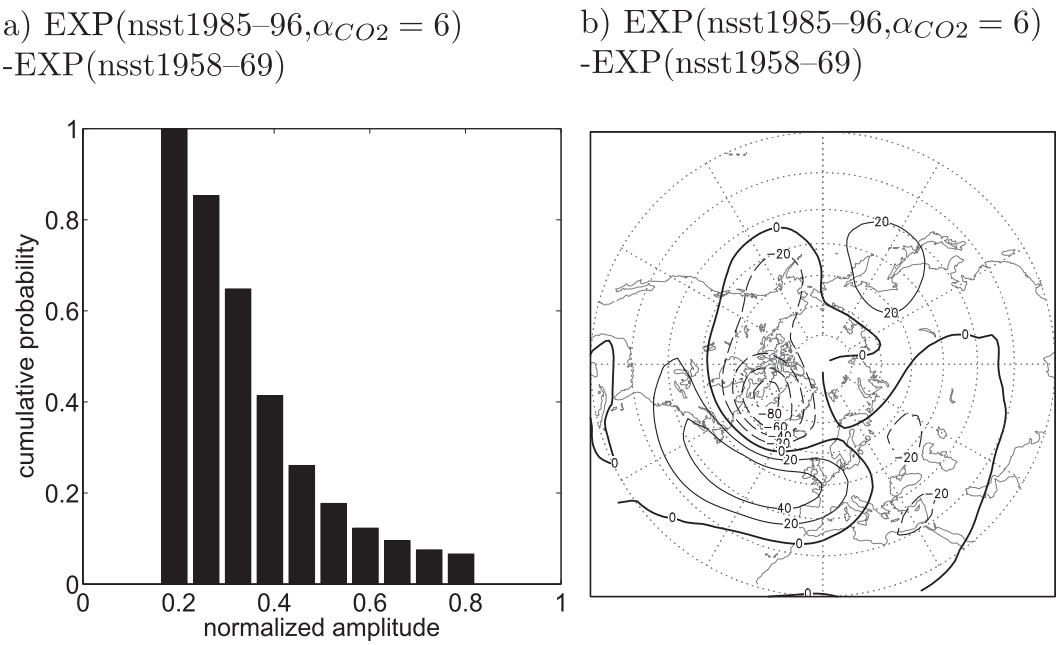

FIG. 7. (a) Cumulative probability (y axis) for members' trend spatial amplitudes (x axis), which are normalized with observed trend spatial amplitude (i.e., radial distances of solid dots in Fig. 6d). (b) DJFM 500-mb geopotential heights trend for a selected member (CI = 20 m). Spatial correlation = 0.97 and normalized spatial amplitude = 0.83 in the North Atlantic sector. If not indicated, $\alpha_{CO2} = 5.0$.

variability in the model atmosphere, the modeled trends still have not achieved a large likelihood of completely explaining the observed trend shown in Fig. 1. Shown in Fig. 7b is one of the best members that reproduced a remarkable normalized amplitude of 0.82 and a spatial correlation of 0.97 with the observed trend in the North Atlantic sector. Note the resemblance of this to Fig. 1 both qualitatively and quantitatively, even the positive 20-m trend over Japan, is obtained precisely. Perhaps the observed trend may be explained with internal variability, although this effect may not be very probable in ICTP AGCM because of the small proportion of members that reached high trend amplitudes.

To obtain an indication of the sea ice effect on the trend in this model, we have made additional experiments with ICTP AGCM coupled to a basic one-category sea ice thermodynamic column model (Bitz and Lipscomb 1999). In these experiments the sea ice model is constrained by observed sea ice fractions in the periods of 1958–69 or 1985–96 from the HadISST dataset. The sea ice model was found to behave reasonably, producing seasonally varying thicknesses with the correct phase (thickest in the early spring, thinnest in early fall), reasonable thicknesses (~280–310 cm near the North Pole), and thickness changes between the seasons (~30 cm). The clearest sea ice trend is found to be the reduction in the seas around Greenland (e.g., see Magnusdottir et al. 2004) and the Bering Sea near Alaska.

A pair of experiments are run with NOAA SST and HadISST sea ice in the corresponding periods, 50-m thermodynamic slab ocean in the Northern Hemisphere, as well as $\alpha_{CO2} = 6.0$ for the period 1985–96 [see EXP(nsst1958–69, SISO) and EXP(nsst1985–96, $\alpha_{CO2} = 0.6$, SISO) in Table 2]. The result is shown in Fig. 8. The inclusion of the simple sea ice model here does not improve the modeled mean trend amplitude or the mean trend correlation with the observed trend. However, there is a small increase in the internal decadal variability of the system, as can be seen in Fig. 8c (cf. with Fig. 7a). This is indicated by the slight increase in the proportion of members attaining higher spatial amplitudes. This result suggests that correct representation of sea ice processes in a climate model may be required to reproduce the desired atmospheric decadal variability. Further studies are required to examine this point rigorously. The total response to an independent forcing by sea ice trend from 1958–69 to 1985–96 actually resembles a negative NAO, as shown in Fig. 9 [also see Magnusdottir et al. (2004) and Deser et al. (2004)].

Next, the effect of solar radiation absorption by stratospheric ozone is investigated. The stratosphere is represented in ICTP AGCM at its two topmost layers at the 100- and 30-mb pressure levels. The fractions of shortwave radiation flux absorbed by these two levels are determined by zonally symmetric functions, which are varying daily, with higher absorption at the poles and

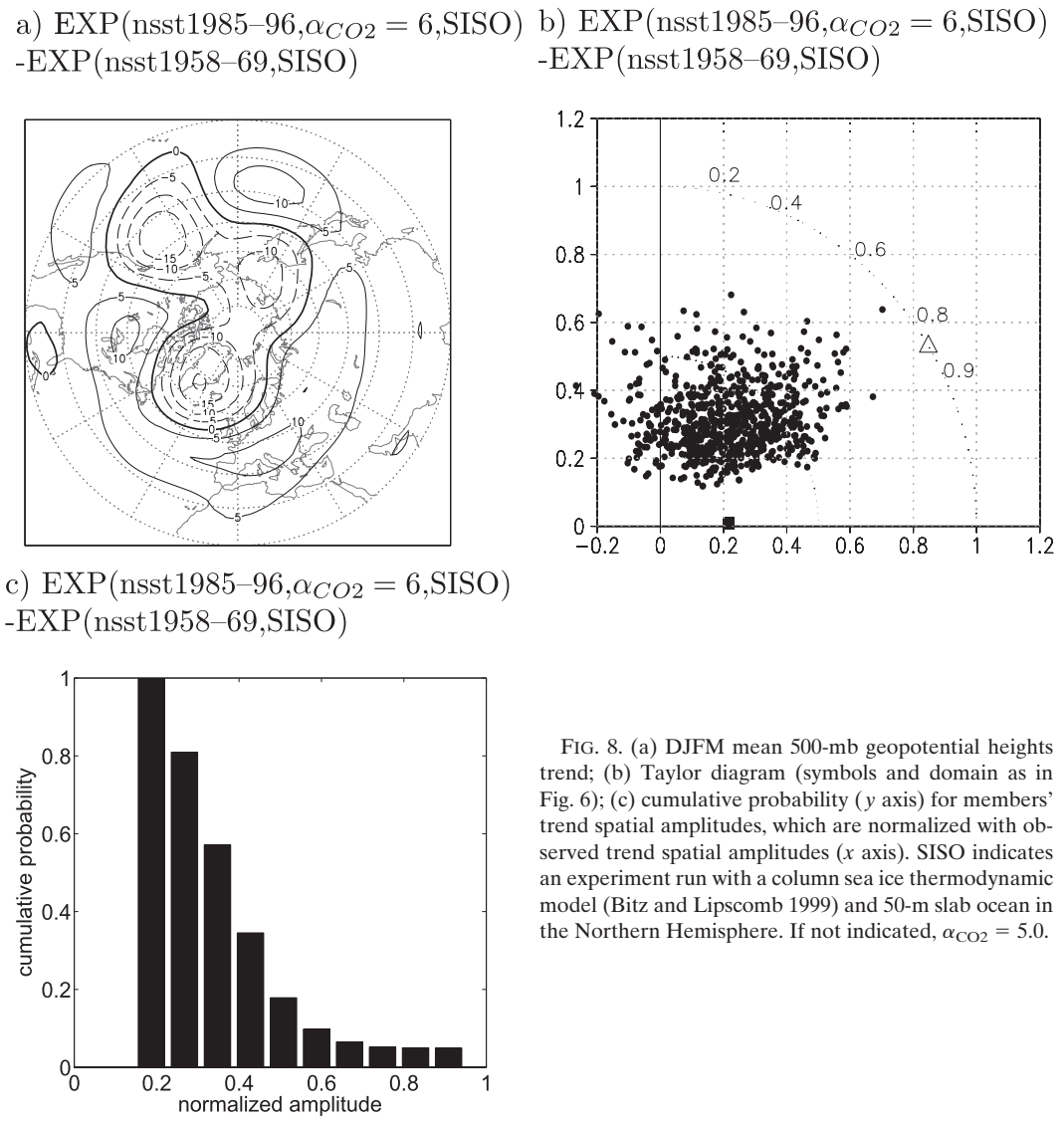

FIG. 8. (a) DJFM mean 500-mb geopotential heights trend; (b) Taylor diagram (symbols and domain as in Fig. 6); (c) cumulative probability (y axis) for members' trend spatial amplitudes, which are normalized with observed trend spatial amplitudes (x axis). SISO indicates an experiment run with a column sea ice thermodynamic model (Bitz and Lipscomb 1999) and 50-m slab ocean in the Northern Hemisphere. If not indicated, $\alpha_{CO2} = 5.0$.

seasonal changes with higher absorption at the winter pole (see Fig. 10). The fractions absorbed are proportional to a parameter named EPSSW, whose default value is tuned to EPSSW = 0.025. The cases investigated in this study result in only very small negative radiative forcings (in the order of -0.1 W m^{-2}), which is comparable to the radiative forcing caused by stratospheric ozone in the last few decades of the twentieth century (Forster et al. 2007).

The maximum damping time for additional diffusion in the ICTP AGCM upper stratosphere is set to 12 h. This value has been tuned to allow the ICTP AGCM top layer to act as a sponge layer. The damping time for drag on zonal-mean wind in the stratosphere is set to 1 month. This value has been tuned for the model to achieve winds climatology, which has good agreement with observation. For the present study, we do not change the above damping times. In essence, the top two levels in ICTP AGCM, rather than being an actual stratospheric model, provide boundary conditions that model the effects of the stratosphere on the troposphere.

To provide an indication for the behavior of the stratospheric flows in the extratropics in ICTP AGCM, shown in Fig. 11 are the scatterplots for the 30-mb geopotential height anomalies, area averaged over the region poleward of 70°N, against the calendar months. The data used are the National Centers for Environmental Prediction–National Center for Atmospheric Research (NCEP–NCAR) reanalysis for 1949–2002 (Fig. 11a); the 20C3M experiment for 1950–99, produced by HadCM3 and CCSM3; and a historical, global SST-forced experiment for 1950–1999 by ICTP AGCM. Thompson and

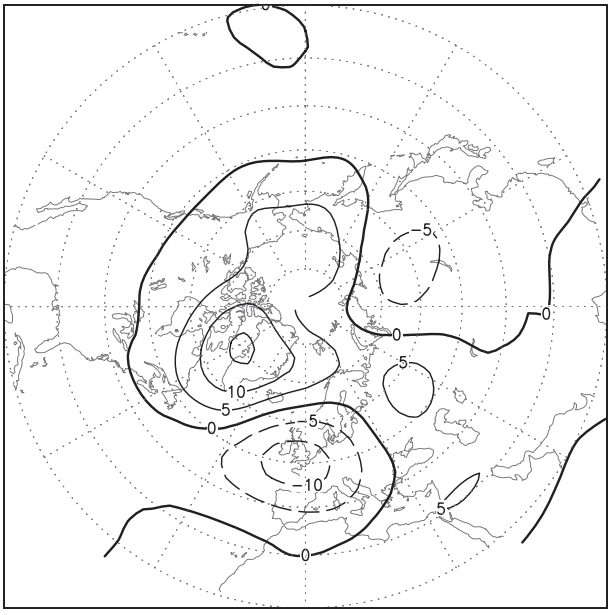

FIG. 9. DJFM mean 500-mb geopotential heights trends by sea ice forcing only. It is forced by observed sea ice trend with the Bitz and Lipscomb (1999) sea ice model.

Wallace (2000) plotted other similar quantities for daily data in the same way (see their Fig. 4). The 20C3M is a CMIP3 climate of the twentieth century coupled-model experiment (further details of the CMIP3 experiment and models are available online at http://www-pcmdi.llnl.gov/ipcc/about_ipcc.php).

In comparison with the NCEP reanalysis, it is observed that the three models capture the seasonality and the strength of the variability very well. In particular, the increased variability in the cold months from November to April is in agreement with the reanalysis data. However, relative to the results from HadCM3 and ICTP AGCM, CCSM3 was able to produce better agreement in having stronger variability over these months. The stratosphere in ICTP AGCM performs reasonably well in this comparison.

Figure 12 shows the results of reducing EPSSW, imitating the slight decrease in stratospheric ozone. The increase in ensemble-mean trend amplitudes and spatial correlations (comparing Taylor diagrams in Fig. 6d and those in Fig. 12) indicate that stratosphere processes play an important role. Experiments with further reduction in EPSSW have shown even better results (e.g., Figure 12f), where the variability among members' trends also have a good likelihood of reproducing the observed amplitudes.

Figures 13a,b show the zonal-mean zonal wind trends from the same experiments of Figs. 12c,e, respectively. The observed zonal-mean zonal wind trend is up to about 7 m s^{-1} in the northern polar stratosphere (Scaife et al. 2005), and for the experiments presented here, up to 6 and 9 m s^{-1}, respectively, are obtained. In Scaife et al. (2005), the reduction in Rayleigh drag was imposed in HadAM3 AGCM to produce up to 8 m s^{-1} of stratospheric zonal wind trend. Therefore, judging by the resulting zonal wind trends obtained in our experiments, the choice of values for EPSSW here are not unacceptable. Note that this zonal wind trend is not obtained by only decreasing the ozone absorption, but rather the pair of responses shown in Fig. 13 includes changes in SST, sea ice, and CO_2 compared to the base experiment.

The desired result of increased amplitude in the spatial trend in the troposphere is robust if the polar jet trend achieves the required magnitude. However, because of the low vertical (and horizontal) resolution of the AGCM used here, it is not known if the mechanism for the stratosphere–troposphere connection that occurs in the model is the same as what had happened during the later half of the twentieth century in the real atmosphere. Also, it is unclear how the stratospheric zonal-mean wind trend can be correctly obtained by models under external forcings but without artificial perturbation, as was done by Scaife et al. (2005) and here.

The dynamics of the stratosphere–troposphere connection in ICTP AGCM can be described briefly using the perspective given here. The responses due to only stratospheric ozone reduction are used for the present explanation. Butler et al. (2010) made a similar observation and discussion. The cooling response in the stratosphere (Fig. 14a) disturbs the zonal wind, through the thermal wind balance, by shifting the jet northward (Fig. 14b) as well as strengthening it. The anomalous u wind affects the poleward eddy momentum flux ($u'v'$, shading in Fig. 14b). In a steady-state condition, we have for the zonal-mean circulation (Holton 2004, 318–324)

$$-f_0 v = -\frac{d(u'v')}{dy},$$

where f_0 is the Coriolis parameter. For our case, $d(u'v')/dy$ is negative (a convergence of eddy momentum fluxes) poleward of around 50°N; therefore, a negative anomalous southward meridional wind v is induced (Fig. 14c, near the top level around 55°N). Through continuity

$$\frac{\partial \omega}{\partial p} = -\frac{\partial v}{\partial y},$$

we have a negative $\partial\omega/\partial p$ (because $\partial v/\partial y$ is positive poleward of around 50°N); thus, a rising motion response is observed in the column above 65°N (Fig. 14d). By an equivalent argument, a sinking motion response is the result in the column above latitudes around 45°N. In this simplistic description, it is seen how a thermal

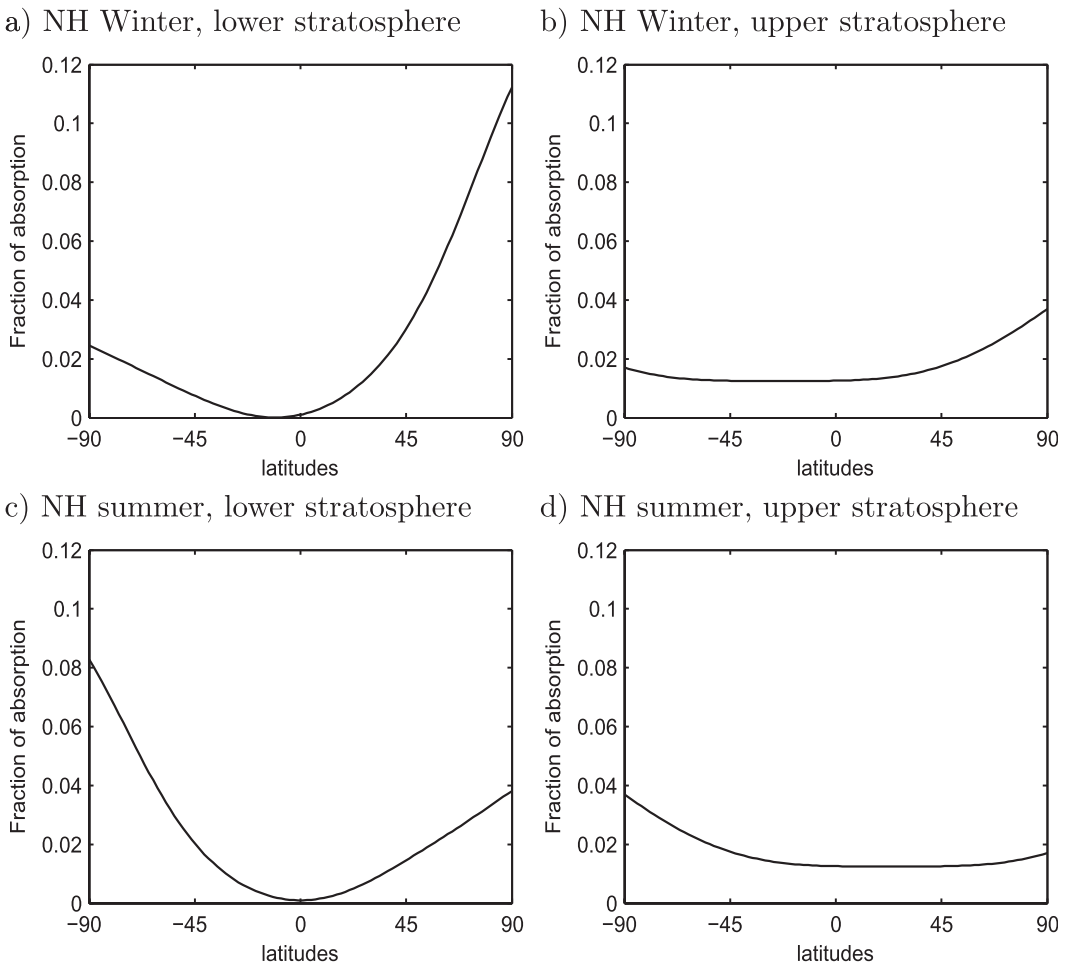

FIG. 10. Zonally symmetric fraction of shortwave radiation flux absorbed by stratospheric ozone against latitudes in ICTP AGCM. The upper stratosphere is set at the 30-mb pressure level; the lower stratosphere at the 100-mb level. The functions depicted here are for selected daily values on Northern Hemisphere winter and summer solstices.

forcing in the stratosphere induces downward propagation of signals into the troposphere.

Last, Fig. 15 shows the trend obtained by an experiment forced with a full set of factors that have been considered in this section (i.e., SST, CO_2, sea ice, and stratospheric ozone). This experiment is marked with an asterisk in Table 2. We consider this set of forcings as the ''best scenario'' forcings among the cases of experiments that we have performed. The spatial correlation with the observed NAO trend is high at nearly 0.9, with a normalized forced trend amplitude of almost 0.4. The hemisphere-wide spatial correlation with the observed trend (Fig. 1) is also high at 0.7. The hemisphere-wide response projects well onto the Arctic Oscillation. The AO response is rather robust in these types of experiments; for example, see the CO_2 doubling experiments using a model with high vertical resolutions performed by Sigmond et al. (2008).

The choice of EPSSW = 0.02 is further justified by the resulting zonal-mean zonal wind trend shown in Fig. 15c, where it has attained up to 7 m s^{-1} in agreement with observation. As mentioned previously, the anomalous radiative forcing by the reduction of ozone absorption of incoming shortwave radiation is in the order of -0.1 W m^{-2}, which is consistent with that reported for this period (Forster et al. 2007). Despite some of the issues discussed above, we argue the results here add to the growing evidence that the stratosphere has an important dynamical effect on the troposphere, even for a model with very low resolution in the stratosphere.

A further reduction in ozone absorption of incoming solar radiation (i.e., by reduction of the EPSWW parameter) may not be justified because of the excessive zonal wind produced. Also, it has been found that the sea ice compensates by becoming thinner and having a warmer surface temperature. This is a direct result of

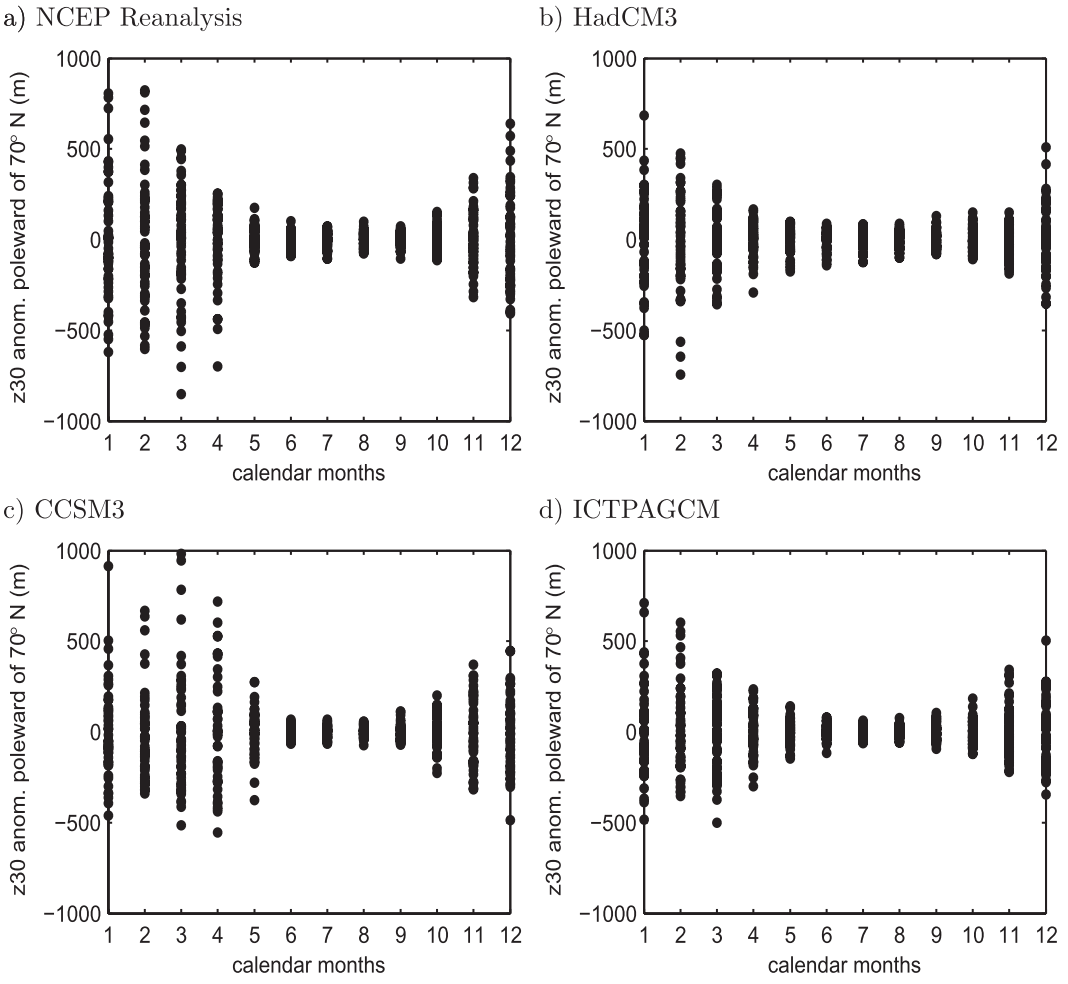

FIG. 11. Monthly-mean 30-mb geopotential height anomalies averaged over the region poleward of 70°N, plotted against the calendar months. The NCEP reanalysis data are for 1949–2002. The HadCM3 or CCSM3 data are obtained from a single run of the CMIP3's 20C3M experiments for the years 1950–99. The ICTP AGCM 50-yr data are from a single run forced with historical global SST from 1950 to 1999 (a pre-1950 2-yr spinup was discarded).

more shortwave radiation reaching the earth's surface because less of it is absorbed by the stratospheric ozone. As in the case shown in Fig. 9, a reduction in sea ice produces a negative NAO trend and therefore limits the tropospheric circulation trend amplitude (i.e., in the presence of sea ice, excessive negative radiative forcing by stratospheric ozone does not help in producing even higher forced trend amplitude of positive NAO).

2) PDFs FOR POSITIVE NAO TRENDS

To obtain a further indication of the roles of internal variability and forced responses, Fig. 16 shows the PDFs for a few selected experiments. The x axis represents positive NAO trends normalized by the observed NAO trend of 1958–69 to 1985–96. The NAO trends are obtained from the trends found in pairs of randomly selected DJFM fields in the two experiments indicated for each PDF. Here, the NAO index is defined as area-averaged SLP in the region 30°–60°N, 90°W–60°E minus that in the area 60°–80°N, 80°–20°W.

The solid curve is the PDF for trends from a single simulation. For this curve, any positive trend found between two randomly selected winters within a single simulation is considered to be due to internal variability, as the external forcings are identical. The mean positive trend by internal variability alone is 0.17 and its 95th percentile (meaning there are only 5% of members having equal and greater amplitudes) is 0.41 (indicated by the left vertical line).

SST forcing alone does not appear to be sufficient (dashed line); adding CO_2 forcing improves the modeled trend (dot–dashed line). Further adding the stratospheric ozone reduction (and the sea ice model), the PDF shifts far to the right (dotted line). Note also that the dotted line

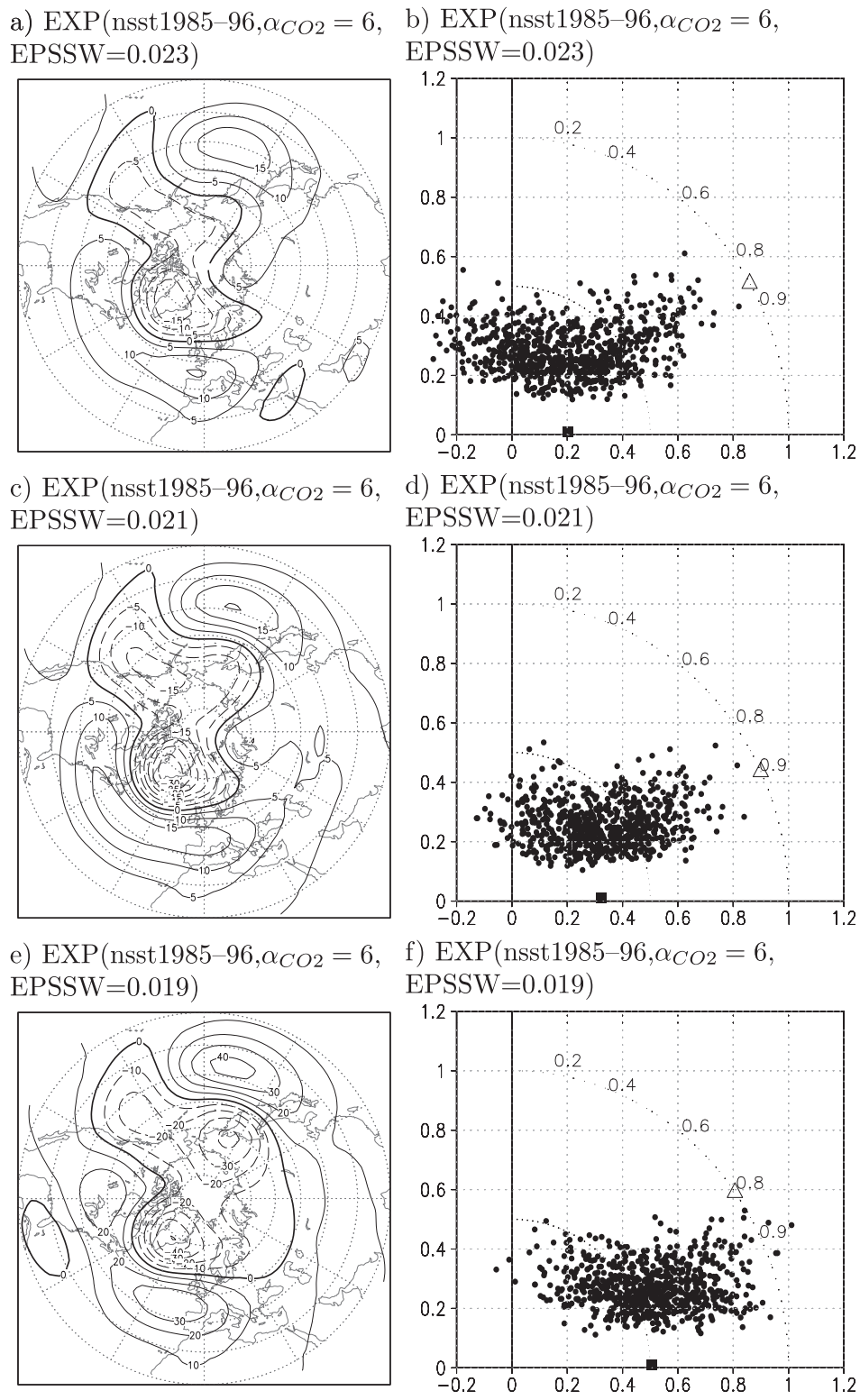

FIG. 12. (a),(c),(e) DJFM 50-mb geopotential heights mean trends; (b),(d),(f) Taylor diagrams (symbols and domain as in Fig. 6). All are relative to the base experiment EXP(nsst1958–69). CI = (a),(c) 5 and (e) 10 m.

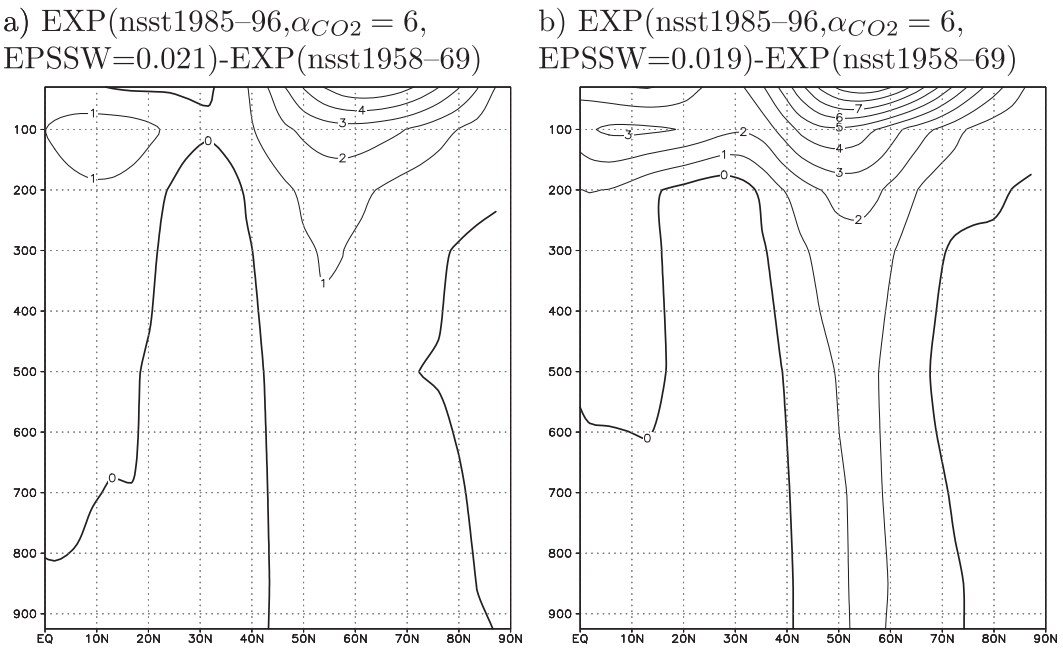

FIG. 13. DJFM zonal-mean u wind trends (CI = 1 m s^{-1}) in the Northern Hemisphere. The observed zonal wind trend in the northern polar stratosphere is 7 m s^{-1}. If not indicated, $\alpha_{CO2} = 5.0$ and EPSSW = 0.025.

represents the best scenario forcings experiment shown in Fig. 15. The best scenario forcings experiment has a normalized mean NAO trend of 0.38 and a 95th percentile of 0.78 (right vertical line). This means that, at the 95th percentile of the trend amplitudes, internal variability contributes ~40% (as in the 95th percentile of the control experiment), while the externally forced component contributes 38% to the observed trend.

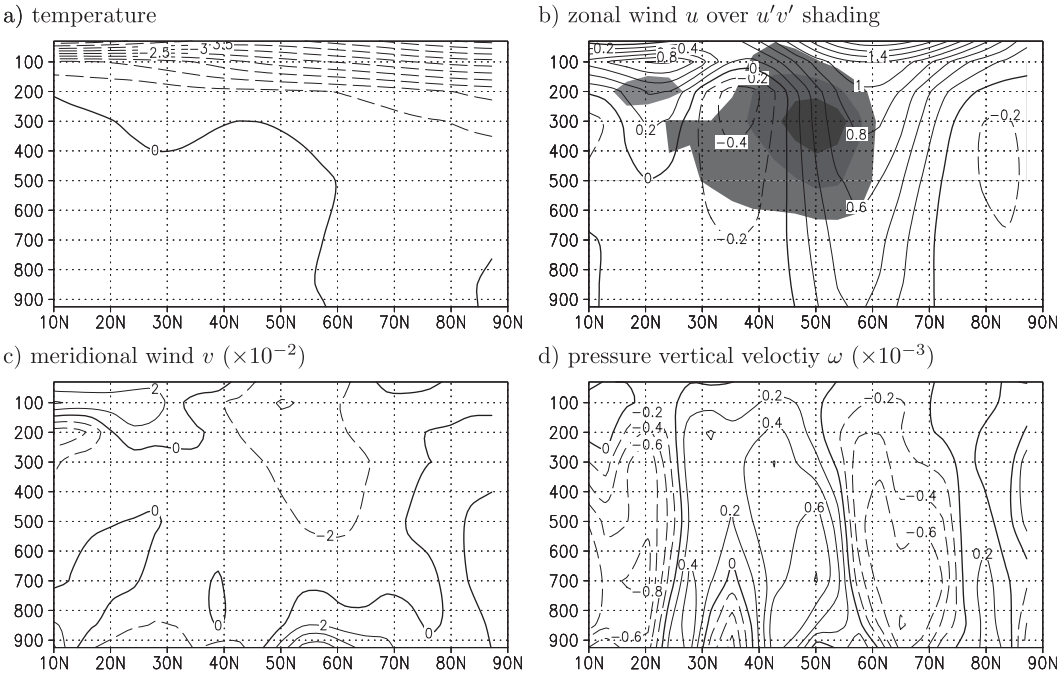

FIG. 14. DJFM zonal-mean responses from EXP(nsst1985–96, EPSSW = 0.02) − EXP(nsst1985–96, EPSSW = 0.025), i.e., the responses are produced by a change in stratospheric ozone only: (a) temperature response (CI = 0.5 K); (b) u contours (CI = 0.2 m s^{-1}) overlay eddy momentum fluxes $u'v'$ shading (CI = 0.5 m^2 s^{-2}); (c) v contours (CI = 0.02 m s^{-1}); and (d) pressure vertical velocity ω (CI = 0.2 × 10^{-3} Pa s^{-1}), where $\omega \approx -\rho g w$.

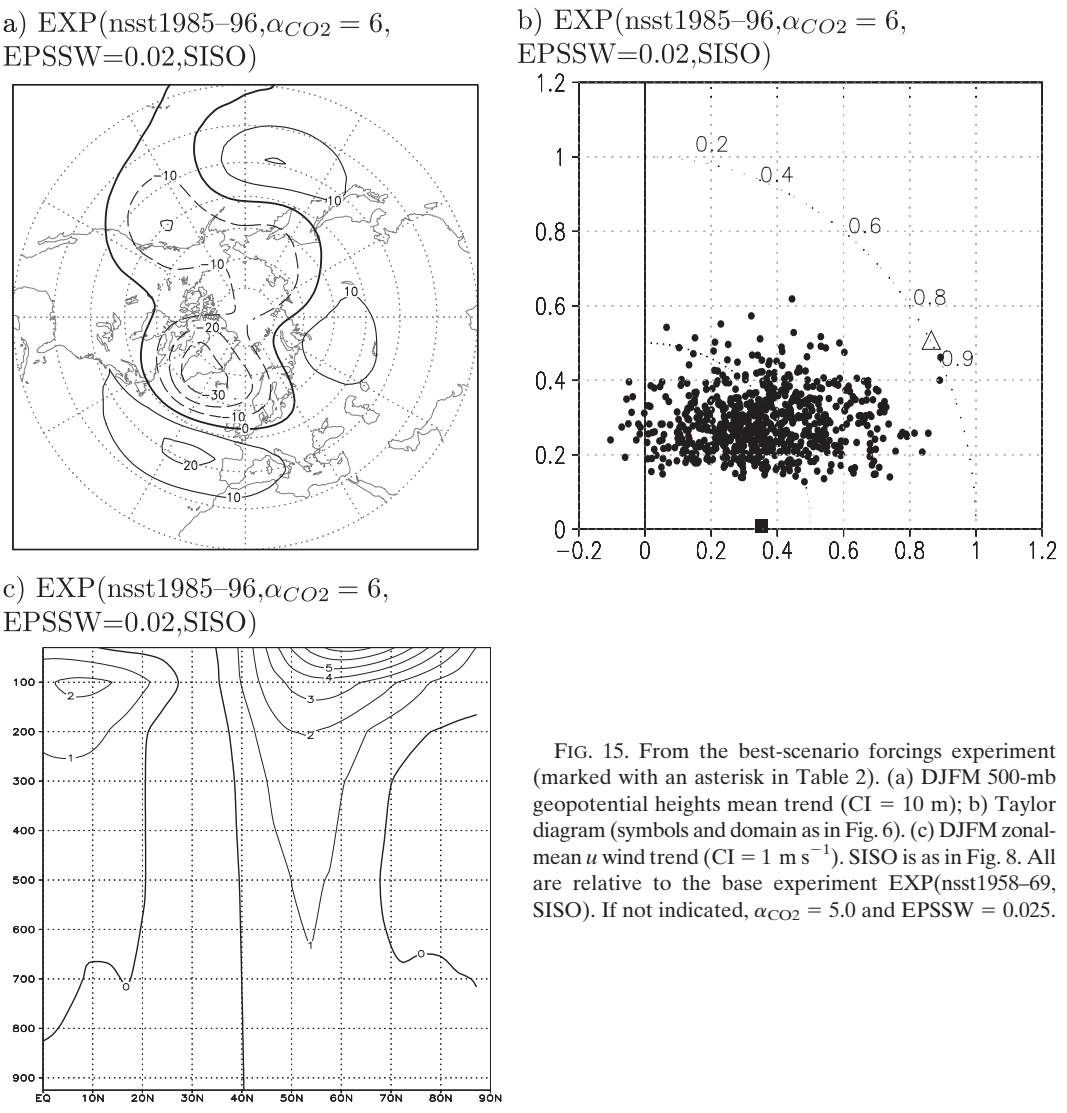

FIG. 15. From the best-scenario forcings experiment (marked with an asterisk in Table 2). (a) DJFM 500-mb geopotential heights mean trend (CI = 10 m); b) Taylor diagram (symbols and domain as in Fig. 6). (c) DJFM zonal-mean u wind trend (CI = 1 m s^{-1}). SISO is as in Fig. 8. All are relative to the base experiment EXP(nsst1958–69, SISO). If not indicated, α_{CO2} = 5.0 and EPSSW = 0.025.

Hurrell et al. (2004) reported that the multimodel GOGA ensemble and the CCM3 TOGA ensemble-mean trends obtained 30% and 40% of the observed trend amplitude (see their Fig. 4). Our SST-forced (without the radiative forcings) trend achieved only about 20% (e.g., see Figs. 4a, 6c) of the observed trend. This is slightly weaker compared to the ensembles used in Hurrell et al. (2004). As in that study, our experiments found none of the members can reach 100% of the observed trend amplitude.

All of the PDFs shown in Fig. 16 have different means relative to the control experiment PDF (solid line) at a statistical significance level of 5% and below using the Welch's t test (similar to Student's t test but for samples with unequal variances). This is possible mainly because of the long sample sizes available from these experiments.

4. Concluding remarks

The main findings and conclusions are summarized below.

From the C20C experiments:

(i) In ICTP AGCM, the modeled North Atlantic 500-hPa changes in the periods from 1958–69 to 1985–96 can be reproduced with forcing by tropical SSTs. The spatial structure is well reproduced (spatial correlation ≈ 0.8) but the amplitudes (≈25% of observed trend amplitudes) are underestimated by the model experiments (Fig. 4b).

(ii) Trend amplitudes are reproduced at most only about 50% of the observed trend by individual ensemble members and only 20%–30% for the ensemble-mean trend.

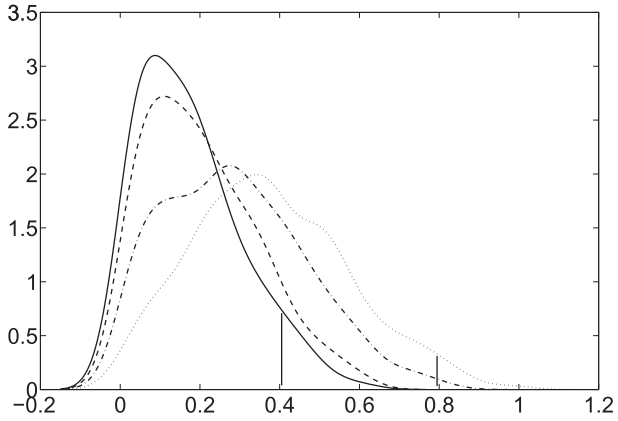

FIG. 16. PDFs for positive NAO normalized trends (normalized by observed trend): Control EXP(nsst1985–96) (solid); EXP(nsst1985–96) − EXP(nsst1958–69) (dashed); EXP(nsst1985–96, $\alpha_{CO2} = 0.6$) − EXP(nsst1958–69) (dot–dashed); and EXP(nsst1985–96, $\alpha_{CO2} = 0.6$, EPSSW = 0.02, SISO) − EXP(nsst1958–69, SISO) (dotted). The two thin vertical lines indicate the 95th percentiles for the control and the best-scenario forcing experiment.

The current study supports the above conclusions by results from relatively large AGCM ensembles with time-dependent historical SST forcings, and inspecting the forced trends and the variabilities in ensembles using Taylor diagrams. The underestimation of the trend amplitude is a common difficulty even for state-of-the-art AGCMs, as well as coupled models with external forcings.

From the idealized experiments:

(i) Change in CO_2 in the periods from 1958–69 to 1985–96 is an important driver, primarily through the forcing of Arctic Oscillation, in contributing to the improvement of amplitudes and correlation in the simulated trend (Figs. 5, 6).
(ii) There is an indication that Arctic sea ice has contributed to the low-frequency internal variability of the system (comparing Fig. 8 with Figs. 6d, 7a), but further study is required to establish this point.
(iii) Stratospheric dynamics and chemistry have played a significant role in increasing both the trend amplitudes and correlations with the observed trend of the troposphere (Fig. 12) However, it has been speculated by Scaife et al. (2005), for example, that a part of the observed stratospheric zonal wind trend itself may be due to internal atmospheric variability, rather than fully externally forced.

The above factors had been separately suggested to be important. The experiments in the present paper highlight that incorporating all of these forcings (and simulating them correctly in a climate model) is crucial for simulating decadal variability and trends. Further studies can be conducted to investigate the interactions among those driving processes and how they affect the atmospheric internal and forced variabilities. The simulated trends may also depend sensitively on how the different drivers produce effects that may combine or cancel (e.g., interactions between stratosphere and sea ice via the troposphere).

The simulated ensemble-mean trends are underestimated by more than 70% in the C20C experiments. Inspecting the members' variabilities among the C20C simulations indicates that it is unlikely the internal atmospheric variability could be the main factor in explaining the observed trend. Taking all of the 130 ensemble members together in the C20C ensembles, not a single member reaches the observed amplitude of the 1958–69 to 1985–96 500-hPa height changes.

From the PDFs in Fig. 16, it is seen that the forced trend contributes about 38% (from the mean NAO trend for the ''best scenario'' forcing, represented by the dotted line in Fig. 16, or $r = 0.38$ for the square in Fig. 15b) to the observed trend amplitude. At the 95th percentile, the total trend is about 78%, meaning that the internal variability contributes about 40%. At the 95th percentile, the simulated trend is still falling short of the observed trend amplitude by about 20%.

Our results appear to be qualitatively consistent with those in Deser and Phillips (2009), who performed CAM3 AGCM ensemble experiment prescribed with SST and radiative forcings (see their Fig. 5b, the ''SST + ATM'' experiment). Prescribing the SST and radiative forcings produce an externally forced NAO trend with an amplitude that is only a portion of the observed trend, and then the internal variability in a small proportion of members is able to bring the total simulated amplitudes close to the observed one.

One valid problem remains: the AGCM used here is not able to capture the amplitude of the observed trend because of ''model deficiencies'' (Hurrell et al. 2004). Another major player in decadal climate variability is the ocean circulation, which is not accounted for at all by the study here. Using an AGCM is a simplification with respect to the fully coupled system. However, it is also an efficient way to include or isolate dominant drivers for the observed trends. Moreover, coupled models have problems of biases and do not reproduce the observed regional SST trends (Deser and Phillips 2009; Kucharski et al. 2009). From the evidence shown in Hurrell et al. (2004), Scaife et al. (2009), and here in Fig. 4e, the trend weakness problem appears to be shared by other AGCMs as well as coupled models.

Acknowledgments. This study is a contribution to the CLIVAR C20C Project (Folland et al. 2002). MPK was supported by an Arctic Region Supercomputing Center

Postdoctoral Fellowship. We also acknowledge the three very constructive and detailed reviews.

REFERENCES

Annamalai, H., H. Okajima, and M. Watanabe, 2007: Possible impact of the Indian Ocean SST on the Northern Hemisphere circulation during El Niño. *J. Climate,* **20,** 3164–3189.

Bader, J., and M. Latif, 2003: The impact of decadal-scale Indian Ocean sea surface temperature anomalies on Sahelian rainfall and the North Atlantic Oscillation. *Geophys. Res. Lett.,* **30,** 2169–2172, doi:10.1029/2003GL018426.

Bitz, C. M., and W. H. Lipscomb, 1999: An energy-conserving thermodynamic model of sea ice. *J. Geophys. Res.,* **104,** 15 669–15 677.

Bracco, A., F. Kucharski, R. Kallummal, and F. Molteni, 2004: Internal variability, external forcing and climate trends in multi-decadal AGCM ensembles. *Climate Dyn.,* **23,** 659–678.

Branstator, G., 2002: Circumglobal teleconnections, the jet stream waveguide, and the North Atlantic Oscillation. *J. Climate,* **15,** 1893–1910.

Butler, A. H., D. W. J. Thompson, and R. Heikes, 2010: The steady-state atmospheric circulation response to climate change-like thermal forcings in a simple general circulation model. *J. Climate,* **23,** 3474–3496.

Deser, C., and A. Phillips, 2009: Atmospheric circulation trends, 1950–2000: The relative roles of sea surface temperature forcing and direct atmospheric radiative forcing. *J. Climate,* **22,** 396–413.

——, G. Magnusdottir, R. Saravanan, and A. Phillips, 2004: The effects of North Atlantic SST and sea ice anomalies on the winter circulation in CCM3. Part II: Direct and indirect components of the response. *J. Climate,* **17,** 877–889.

Folland, C. K., J. Shukla, J. Kinter, and M. J. Rodewell, 2002: Climate of the twentieth century project. *CLIVAR Exchanges,* No. 7, International CLIVAR Project Office, Southampton, United Kingdom, 37–39.

Forster, P. V., and Coauthors, 2007: Changes in atmospheric constituents and in radiative forcing. *Climate Change 2007: The Physical Science Basis,* S. Solomon et al., Eds., Cambridge University Press, 129–234.

Gerber, E. P., and L. R. Polvani, 2009: Stratosphere–troposphere coupling in a relatively simple AGCM: The importance of stratospheric variability. *J. Climate,* **22,** 1920–1933.

Gill, A., 1980: Some simple solutions for heat-induced tropical circulations. *Quart. J. Roy. Meteor. Soc.,* **106,** 447–462.

Gillett, N. P., M. R. Allen, and K. D. Williams, 2002: The role of stratospheric resolution in simulating the Arctic Oscillation response to greenhouse gases. *Geophys. Res. Lett.,* **29,** 1500, doi:10.1029/2001GL014444.

Hoerling, M. P., J. W. Hurrell, and T. Xu, 2001: Tropical origins for recent North Atlantic climatic change. *Science,* **292,** 90–92.

——, ——, ——, G. T. Bates, and A. S. Philips, 2004: Twentieth century North Atlantic climate change. Part II: Understanding the effect of Indian Ocean warming. *Climate Dyn.,* **23,** 391–405.

Holton, J. R., 2004: *An Introduction to Dynamic Meteorology*. 4th ed. Elsevier Academic Press, 535 pp.

Hoskins, B., and D. Karoly, 1981: The steady linear response of a spherical atmosphere to thermal and orographic forcing. *J. Atmos. Sci.,* **38,** 1179–1196.

Hurrell, J. W., 1995: Decadal trends in the North Atlantic Oscillation: Regional temperature and precipitation. *Science,* **269,** 676–679.

——, M. P. Hoerling, A. S. Philips, and T. Xu, 2004: Twentieth century North Atlantic climate change. Part I: Assessing determinism. *Climate Dyn.,* **23,** 371–390.

Jin, F.-F., and B. J. Hoskins, 1995: The direct response to tropical heating in a baroclinic atmosphere. *J. Atmos. Sci.,* **52,** 307–319.

Kalnay, E., and Coauthors, 1996: The NCEP/NCAR 40-Year Reanalysis Project. *Bull. Amer. Meteor. Soc.,* **77,** 437–471.

King, M. P., and F. Kucharski, 2006: Observed low-frequency covariabilities between the tropical oceans and the North Atlantic Oscillation in the twentieth century. *J. Climate,* **19,** 1032–1041.

Kucharski, F., F. Molteni, and A. Bracco, 2006: Decadal interactions between the western tropical Pacific and the North Atlantic Oscillation. *Climate Dyn.,* **26,** 79–91.

——, and Coauthors, 2009: The CLIVAR C20C project: Skill of simulating Indian monsoon rainfall on interannual to decadal timescales. *Climate Dyn.,* **33,** 615–627.

Lin, H., and J. Derome, 2004: Nonlinearity of the extratropical response to tropical forcing. *J. Climate,* **17,** 2597–2608.

Lu, J., R. J. Greatbatch, and K. A. Peterson, 2004: Trend in Northern Hemisphere winter atmosphere circulation during the last half of the twentieth century. *J. Climate,* **17,** 3745–3760.

Magnusdottir, G., C. Deser, and R. Saravanan, 2004: The effects of North Atlantic SST and sea ice anomalies on the winter circulation in CCM3. Part I: Main features and storm track characteristics of the response. *J. Climate,* **17,** 857–876.

Manganello, J. V., 2007: The influence of sea surface temperature anomalies on low-frequency variability of the North Atlantic Oscillation. *Climate Dyn.,* **30,** 621–641.

Marshall, J., and Coauthors, 2001: North Atlantic climate variability: Phenomena, impacts and mechanisms. *Int. J. Climatol.,* **21,** 1863–1898.

Mehta, V. M., M. J. Suarez, J. V. Manganello, and T. L. Delworth, 2000: Oceanic influence on the North Atlantic Oscillation and associated Northern Hemispheric climate variations: 1959–1993. *Geophys. Res. Lett.,* **27,** 121–124.

Molteni, F., 2003: Atmospheric simulations using a GCM with simplified physical parameterizations. I: Model climatology and variability in multi-decadal experiments. *Climate Dyn.,* **20,** 175–191.

Polvani, L. M., and P. J. Kushner, 2002: Tropospheric response to stratospheric perturbations in a relatively simple general circulation model. *Geophys. Res. Lett.,* **29,** 1114, doi:10.1029/2001GL014284.

Rayner, N. A., D. E. Parker, E. B. Horton, C. K. Folland, L. V. Alexander, D. P. Rowell, E. C. Kent, and A. Kaplan, 2003: Global analyses of sea surface temperature, sea ice, and night marine air temperature since the late nineteenth century. *J. Geophys. Res.,* **108,** 4407, doi:10.1029/2002JD002670.

Rodwell, M. J., D. P. Rowell, and C. K. Folland, 1999: Oceanic forcing of the wintertime North Atlantic Oscillation and European climate. *Nature,* **398,** 320–323.

Scaife, A. A., J. R. Knight, G. K. Vallis, and C. K. Folland, 2005: A stratospheric influence on the winter NAO and the North Atlantic surface climate. *Geophys. Res. Lett.,* **32,** L18715, doi:10.1029/2005GL023226.

——, and Coauthors, 2009: The CLIVAR C20C project: Selected twentieth century climate events. *Climate Dyn.,* **33,** 603–614.

Schneider, E. K., L. Bengtsson, and Z. Hu, 2003: Forcing of Northern Hemisphere climate trends. *J. Atmos. Sci.,* **60,** 1504–1521.

Shindell, D. T., R. Miller, G. Schmidt, and L. Pandolfo, 1999: Simulation of recent northern winter climate trends by greenhouse-gas forcing. *Nature,* **399,** 452–455.

Sigmond, M., J. F. Scinocca, and P. J. Kushner, 2008: Impact of the stratosphere on tropospheric climate change. *Geophys. Res. Lett.,* **35,** L12706, doi:10.1029/2008GL033573.

Simmons, A. J., J. M. Wallace, and G. W. Branstator, 1983: Barotropic wave propagation and instability, and atmospheric teleconnection patterns. *J. Atmos. Sci.,* **40,** 1363–1392.

Smith, T. M., and R. W. Reynolds, 2004: Improved extended reconstruction of SST (1854–1997). *J. Climate,* **17,** 2466–2477.

Sterl, A., and W. Hazeleger, 2005: The relative roles of tropical and extratropical forcing on atmospheric variability. *Geophys. Res. Lett.,* **32,** L18716, doi:10.1029/2005GL023757.

Sutton, R. T., and D. L. R. Hodson, 2003: Influence of the ocean on North Atlantic climate variability. *J. Climate,* **16,** 3296–3313.

Taylor, K. E., 2001: Summarizing multiple aspects of model performance in a single diagram. *J. Geophys. Res.,* **106,** 7183–7192.

Thompson, D. W. J., and J. M. Wallace, 2000: Annular modes in the extratropical circulation. Part I: Month-to-month variability. *J. Climate,* **13,** 1000–1016.